



Enhancing the Hydrophobicity and Surface Roughness of Synthesized PVDF Membrane Using Evaporation and Non-solvent-Induced Phase Separation

Meenakshi Yadav¹ · Sushant Upadhyaya¹ · Kailash Singh¹

Received: 7 July 2023 / Accepted: 8 January 2024 / Published online: 21 February 2024
© King Fahd University of Petroleum & Minerals 2024

Abstract

This study focuses on the synthesis of a PVDF membrane using DMAc as the solvent through a combination of evaporation-induced phase separation (EIPS) and non solvent-induced phase separation (NIPS) techniques. The experimental findings underscore the significant role of thermodynamic and kinetic parameters in the phase inversion process, influencing the surface and transport properties of the resulting membrane. By precisely controlling the combined processes of EIPS and NIPS, a customized membrane with specific characteristics such as a rough surface (roughness of up to 725.9 μm) and hydrophobicity (water contact angle up to 117°) was successfully achieved. The synthesized membrane exhibits good membrane properties (total porosity $\geq 50\%$, mean pore size ranging from 0.01 to 0.35 μm) with well-connected pores. To assess its quality, the membranes permeate flux, reaching up to 12.8 $\text{kg h}^{-1} \text{m}^{-2}$, and salt rejection rate of 99.8% were evaluated using Vacuum Membrane Distillation (VMD). Furthermore, a fouling study was conducted to investigate the impact of operating time on membrane performance, revealing a negligible decline in membrane fouling over a 200-h run.

Keywords Phase inversion · Polyvinylidene fluoride (PVDF) · Hydrophobicity · Desalination · Vacuum membrane distillation (VMD)

1 Introduction

The availability of high-quality water is a critical environmental concern in many regions worldwide due to the increasing global population. To meet the demand for freshwater resources, efficient and environmentally friendly water treatment technologies are necessary. Among various water treatment processes, membrane-based separation methods have gained prominence due to their inherent advantages, including easy cleanability, scalability, and mild operating conditions, which contribute to cost-effectiveness and adaptability [1, 2].

Membrane distillation (MD) has emerged as a promising technology for desalination, offering notable features such as high separation efficiency [3], low energy consumption [4], and low operating pressure [5]. In MD processes, the driving

force for separation is the vapor pressure difference across a micro-porous hydrophobic membrane, which allows only vapor molecules to pass through to the permeate side of the membrane module. In achieving stable flux and improved rejection performance, various membrane properties play a crucial role, including hydrophobicity, wetting characteristics, liquid entry pressure (LEP), membrane porosity, pore size distribution, and surface morphology. Understanding the phenomena involved in membrane preparation is essential for obtaining membranes with desired characteristics that ensure long-term sustainability.

In the field of membrane distillation (MD), poly(vinylidene) fluoride (PVDF) has emerged as the preferred material for hydrophobic membranes due to its excellent properties, including chemical and mechanical resistance, which make it well-suited for MD applications [6, 7]. Among the various methods used to fabricate PVDF membranes, the phase inversion technique is widely employed [8, 9]. This technique encompasses four categories: non-solvent-induced phase separation (NIPS), evaporation-induced phase separation (EIPS), thermally-induced phase separation (TIPS), and vapor-induced phase

✉ Sushant Upadhyaya
supadhyay.chem@mmit.ac.in

¹ Department of Chemical Engineering, Malaviya National Institute of Technology, Jaipur 302017, India



separation (VIPS). Of these methods, NIPS is favored for its simplicity and ability to produce membranes with desired properties.

NIPS-prepared membranes possess an asymmetrical and porous structure. Some researchers have successfully enhanced membrane porosity by incorporating additives into the dope solution. Surface modification techniques have also been employed to increase the membrane's hydrophobicity. In MD applications, it is crucial for the membrane to be hydrophobic to prevent the passage of liquid feed, allowing only vapors to pass through [10]. A hydrophobic membrane exhibits non-wettability, even under high flow rates and pressures. The non-wetting behavior can be characterized by the liquid entry pressure (LEP), which depends on factors such as the contact angle of water with the membrane surface, as well as the pore structure and size. The surface roughness of the membrane significantly influences the contact angle (hydrophobicity) of water on the membrane surface. By adjusting the operating parameters during membrane preparation, the surface roughness can be enhanced.

It's worth noting that limited research has ventured into the combination of the two-phase inversion processes for synthesizing PVDF-DMAc membranes [11, 12]. While some authors have tinkered with process parameters, such as brief exposure times to ambient air (ranging from 0.5 to 6 min) before NIPS, however, they have not controlled the environmental humidity [8, 13, 14]. This brief exposure to the atmosphere primarily affects the membrane's surface but cannot be considered as EIPS process. During this short period, it basically promotes solvent evaporation, resulting in a thin skin layer rather than the formation of a porous structure dominated by water vapor diffusion from the atmosphere. The implementation of the prolonged EIPS method before the NIPS process can profoundly impact the membrane's surface characteristics and hydrophobicity. Therefore, in this study, combination of EIPS and NIPS methods has been explored in order to understand the process dynamics for improving the membrane characteristics and hydrophobicity. This research mainly focuses on synthesizing PVDF membranes using a controlled two-phase inversion process, namely EIPS and NIPS. The casted membranes undergo short to prolonged evaporation times during the EIPS method prior to NIPS and its effect on the membrane's morphology, topography, mean pore diameter, membrane porosity, contact angle and transmembrane flux were investigated thoroughly. In addition, fouling study on the membrane surface is also conducted in long run. The main of this work is to contribute systematic knowledge and determining the favorable condition of EIPS prior to NIPS during fabrication of PVDF membrane suitable for desalination application using Vacuum membrane distillation in long usage.

2 Material and Methods

2.1 Materials

Polyvinyl difluoride (PVDF) powder (FR- 904 grade, Kynar HSV 900) was obtained from Sita Chemicals Pvt. Limited in India. The solvent used, dimethyl-acetamide (DMAc), was sourced from TECH INC India Pvt. Limited with a purity of 99.5% and a density of 0.940 g/ml. A non-woven fabric sheet, 100 μm thick, was utilized as the membrane support and was supplied by Permonics Membrane Pvt. Ltd in Vadodara, Gujarat, India.

2.2 Solubility Parameter

The dissolution of a polymer in a solvent is primarily influenced by the Hansen solubility parameter [15]. Hansen's solubility parameter (R_a) comprises three components: the polar component (δ_d), the dispersion force component (δ_p), and the hydrogen bonding component (δ_h). The value of R_a , determined by Eq. 1, represents the distance between the polymer molecule and the solvent molecule. A lower R_a value indicates better solubility of the polymer in the solvent.

$$R_a = \sqrt{4(\delta_{d1} - \delta_{d2})^2 + (\delta_{p1} - \delta_{p2})^2 + (\delta_{h1} - \delta_{h2})^2} \quad (1)$$

where, subscripts 1 and 2 refer to the solvent and the polymer, respectively.

2.3 Preparation of Dope Solution

PVDF flat sheet membranes were synthesized using the dry-wet phase inversion method. To prepare the casting solution for membrane fabrication, PVDF powder (16 wt%) was dissolved in the solvent DMAc (Dimethyl-acetamide). The mixture of DMAc and PVDF powder was stirred at 70 °C using a temperature-controlled magnetic stirrer to achieve a homogeneous dope solution. The resulting solution was then degassed to remove any trapped air. A non-woven fabric was affixed to a glass plate to provide a smooth surface for membrane casting. The homogeneous dope solution was poured onto the non-woven fabric, ensuring even distribution. A membrane casting machine was employed to cast a uniform and thin layer of the polymeric solution, resulting in a film thickness of 250 microns over the non-woven fabric. Following the preparation of the polymeric films, they were placed in a BOD incubator under specific conditions as outlined in Table 1 for the evaporation-induced phase separation (EIPS) process of phase inversion. The incubation was conducted at a temperature of 30 °C and a relative humidity of

Table 1 Nomenclature of membrane prepared with different Evaporation time during EIPS

Membrane code	Evaporation time (min)
M-1	1
M-10	10
M-20	20
M-40	40

30%. This allowed for controlled evaporation of the solvent within the film. Subsequently, the prepared film underwent the non-solvent-induced phase separation (NIPS) process by immersion in a water bath. The film was submerged in the water bath for 24 h to ensure complete solvent removal from the membrane matrix. After the phase inversion processes, the membranes were dried at room temperature for one day and then subjected to further characterization.

2.4 Membrane Characterizations

The synthesized membranes with different evaporation times were subjected to comprehensive characterization to evaluate their morphology, hydrophobicity, crystallinity, surface roughness, tensile strength, porosity, and permeability. The characterization techniques employed included field-emission scanning electron microscopy (FESEM) for morphological analysis, the sessile drop method to determine hydrophobicity, Fourier transform infrared spectroscopy (FTIR) for assessing crystallinity, atomic force microscopy (AFM) to measure surface roughness, universal testing machine (UTM) for tensile strength evaluation, gravimetric method to determine membrane porosity, and Vacuum Membrane Distillation (VMD) for measuring membrane permeability. These techniques provided valuable insights into the membrane’s structural and functional properties, enabling a comprehensive understanding of their performance.

2.4.1 Gravimetric Method

The porosity of the synthesized membrane was determined by the gravimetric method. A square coupon of dimension 1 × 1 cm was cut and submerged in propanol for 24 h at room temperature so that the solvent could penetrate completely inside the pores of the membrane. The weight of the wet and dry samples was measured and the porosity of the membrane was calculated by using Eq. 2 [16]:

$$\epsilon_m = \frac{\frac{W_1 - W_2}{d_i}}{\frac{W_1 - W_2}{d_i} + \frac{W_2}{d_p}} \tag{2}$$

where is the W_1 weight of the wet membrane, g; W_2 is the weight of the dry membrane, g; d_i is the 2-propanol density, g/m³; d_p is the polymer density, g/m³.

2.4.2 Scanning Electron Microscopy (SEM) and ImageJ Software

Scanning electron microscope (SEM) images of the PVDF membranes were obtained to examine their top and cross-sectional views. For the cross-sectional analysis, the membranes were fractured using liquid nitrogen. To enhance conductivity, all PVDF membranes were coated with a thin layer of gold. The gold-coated membranes were then placed on a copper holder and observed under the scanning electron microscope (JEOL, JEM 2100). Multiple SEM images were captured at different magnifications to examine the membrane morphology.

To analyze the SEM images, ImageJ software was utilized. The software was employed to determine the pore size distribution and calculate the mean pore size. The equivalent diameter of the membrane pores was determined based on the estimated area obtained through image processing. The circular assumption was made for the pores, and the calculation was performed using the formula presented in Eq. 3 [17, 18],

$$d_{eq} = \sqrt{A/\pi} \tag{3}$$

The pore size distribution for synthesized membranes was obtained in the form of a histogram and probability density function (pdf) estimated by Eq. 4 [19]:

$$\frac{df(d_m)}{d(d_m)} = \frac{\exp\left\{\frac{-(\ln d_m - \ln \mu_m)^2}{2(\ln \sigma_m)^2}\right\}}{d_m \ln \sigma_m \sqrt{2\pi}} \tag{4}$$

where, d_m is the membrane pore size, σ_m is the geometric standard deviation and μ_m is the mean pore size.

2.4.3 Hydrophobicity and LEP

Hydrophobicity of the fabricated membrane was determined by measuring the contact angle of the dry PVDF membranes using the Sessile drop method. In this method, Kruss Drop shape analyzer (DSA25) Mk2 was used to analyze the contact angle, and a droplet of 4 μl of double distilled water was placed onto the membrane’s top surface with the help of a needle. Afterward, a static image of the water droplet on the membrane surface was taken. Contact angles were measured using FTA software for each membrane at ten different locations.

The liquid entry pressure of water (LEP_w), was defined as the maximum pressure difference at which the first drop

of liquid water penetrates into the pores of the membrane. This is calculated by a theoretical expression, based on the Young Laplace equation, Eq. 5:

$$\text{LEP}_w = \frac{-2\beta\gamma\cos\theta}{r_{\max}} \quad (5)$$

where γ is water surface tension, θ is the contact angle of water to the membrane surface, r_{\max} is the maximum pore radius detected and β is the geometrical factor for the circularity of pores varying from 0 to 1 (1 = for circular pores).

2.4.4 Fourier Transforms Infrared Spectroscopy (FTIR)

The PVDF crystal phase in fabricated membranes was analyzed by FTIR spectra using a PerkinElmer, G-FTIR instrument with a resolution of 0.5. The top layers of the dry membranes were pressed firmly against the crystal plate, and the FTIR spectrum was generated with a spectrum frequency range from 400 to 4000 cm^{-1} . Two replicates from each membrane sample were measured.

2.4.5 Atomic Force Microscopy (AFM)

The surface roughness of the fabricated membrane was measured using an atomic force microscope Bruker Nano 5 AFM setup at Material Research Center, MNIT Jaipur, operated in tapping mode using commercially available Si cantilevers (300 kHz frequency). The force constant of the cantilevers was kept to be 40 N/m, and the cantilever's oscillation frequency was 300 kHz. The scan size of each sample was $5 \times 5 \mu\text{m}$ with a scan rate of 1.0 Hz. At least two replicates were analyzed for each membrane sample.

2.4.6 Mechanical Properties

Mechanical properties of the prepared membranes were measured using Universal Testing Machine (UTM, Instron-5967) at room temperature. The sample was prepared by cutting the membrane samples in rectangular strips of dimension 10 cm \times 2 cm, with a margin of 1.5 cm on both sides to clamp the sample in the machine. These samples were clamped at both ends and pulled in tension at a constant elongation rate of 10 m/min, gauge length 50 mm, and maximum force 250 N. For each condition used, the average values of three replicates were reported.

2.5 Membrane Flux and Salt Rejection

All the prepared membranes were tested on vacuum membrane distillation (VMD) set up for desalination. The membranes were cut into a circular shape ($\phi = 90 \text{ mm}$ with ϕ_e

= 52 mm) to fit in the VMD membrane module. The average permeate flux was determined after a 6-h run at constant operating parameters of feed flow rate, feed temperature, feed salt concentration, vacuum pressure, and chilling temperature. The permeate flux is measured by the following Eq. 6 [20]:

$$N = \frac{\rho \times V \times 10^{-6}}{A \cdot t} \quad (6)$$

where ρ is the density of permeate in kg/m^3 , V is the volume collected in the permeate receiver in ml, A is the effective membrane area ($= \frac{\pi\phi_e^2}{4}$) in m^2 , ϕ_e is the effective diameter in m, t is the time of permeate collection in h, and N is the permeate flux in $\text{kg/m}^2 \cdot \text{h}$.

The salt (NaCl) concentration in the permeate flux was determined by estimating the electrical conductivity of the permeate and by using the calibration curve drawn between salt concentration and conductivity. The salt rejection was calculated by using Eq. 7 [21]:

$$\text{Salt rejection } R(\%) = \left(1 - \frac{C_p}{C_f}\right) \times 100 \quad (7)$$

where C_p and C_f are the salt concentrations in the feed and permeate streams, respectively.

3 Results and Discussions

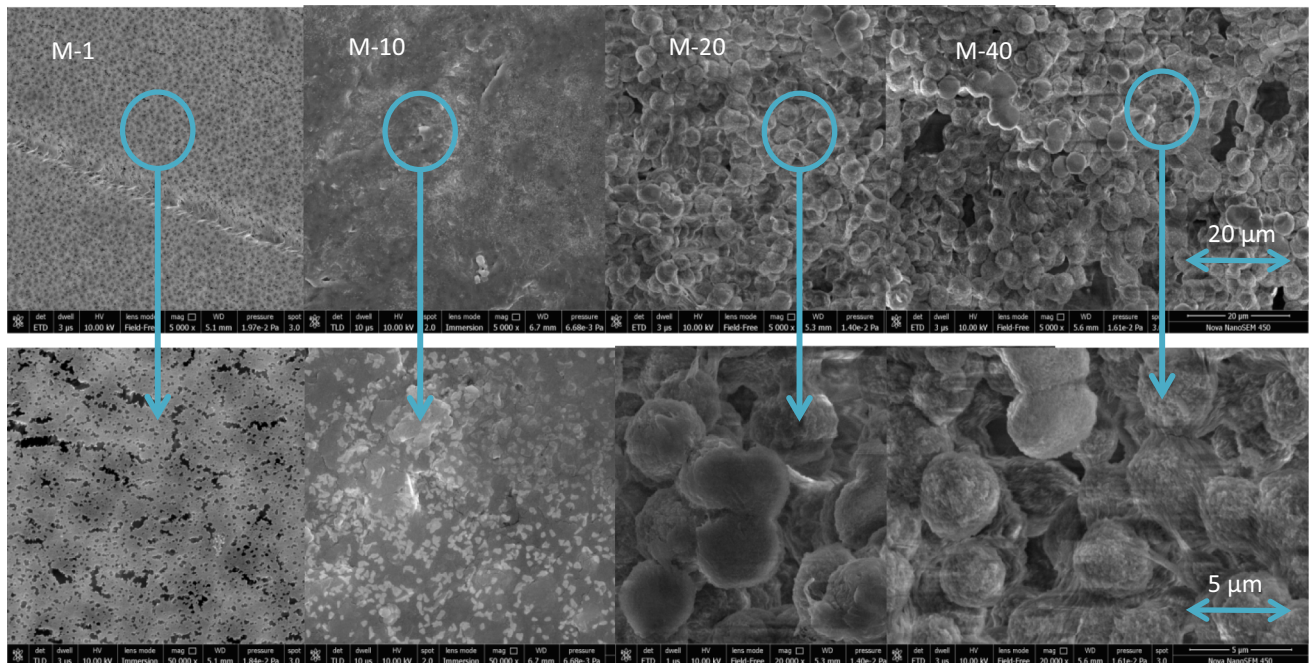
The fabricated membrane topography, morphology, crystalline phase, wetting characteristics, porosity, and mechanical properties are investigated thoroughly by implementing two steps in phase inversion process. Primarily, the effect of evaporation time during EIPS process on membrane characteristics is understood by using various analytical techniques such as AFM, SEM, FTIR, sessile drop method, gravimetric method, and UTM. The scientific findings are discussed in detail in the subsequent sections.

3.1 Solubility

The solubility parameter of four different polar solvents DMAc, NMP, DMSO and DMF was listed in Table 2. It was observed that the value of R_a the solvent – polymer pair of DMAc and PVDF is smaller than those of other solvents, indicating that the affinity of PVDF with DMAc is better than other solvents, so DMAc is considered to be the best solvent to dissolve PVDF.

Table 2 Solubility parameter of solvents with PVDF

Name of solvent	δd	Δp	Δh	$R_a(\text{Solvent-PVDF})$
DMAc	16.8	11.5	10.2	1.624807681
NMP	18	12.3	7.2	2.569046516
DMSo	18.4	16.4	10.2	4.687216658
DMF	17.4	13.7	11.3	2.451530134
PVDF	17.2	12.5	9.2	

**Fig. 1** SEM images of the top surface of PVDF membrane prepared with different EIPS evaporation times at 5000 X(top) and 25,000 X (bottom) magnification

3.2 Topographical Study

Numerous SEM top surface micrographs for casted membranes were captured as shown in Fig. 1. Four sets of micro-graphs are studied under an EIPS evaporation time range of 1–40 min, with magnification of 5000X and their magnified image is also shown in the same image at 20000X. It is observed from Fig. 1 that membrane with an evaporation time of 1 min has smooth and dense surface containing numerous pores in it. This morphology results when NIPS dominates the phase inversion process where there is a rapid exchange of solvent and non-solvent at the time of demixing. As the casted polymeric film was dipped in the coagulation bath, immediately the phase separation began with the movement of solvent out from the membrane matrix and non-solvent inwards the membrane matrix. The membrane matrix is divided into two phases: one with the higher polymer concentration that forms the solid part of the membrane, and another phase with the lower polymer concentration that gives rise to the pores. The movement of solvent from

the membrane matrix toward the top surface increases the polymer concentration at the top surface forming a thin polymeric layer at the top which acts as a mass transfer barrier for solvent and non-solvent exchange rate. An asymmetrical structure with a thin porous skin layer at the top, followed by a finger-like structure, and underneath a sponge-like structure was formed with EIPS evaporation time of one minute. When the EIPS evaporation time increased to 10 min a noticeable change was observed in the SEM image of the M-10 membrane depicted in Fig. 1. Some small structures embedded in the membrane matrix are visible showing the nucleation of polymer PVDF. The nucleation of polymer can be explained by the fact that the humidity present in the environment causes instantaneous phase inversion of polymeric film at some particular points resulting in the formation of small globules at the membrane's top surface. The formation of these globules on the top skin of the casted membrane may increase the membrane roughness and reduce the membrane-wetting characteristics. From Fig. 2, it is observed that the cross-sectional structure of the membrane is asymmetric in

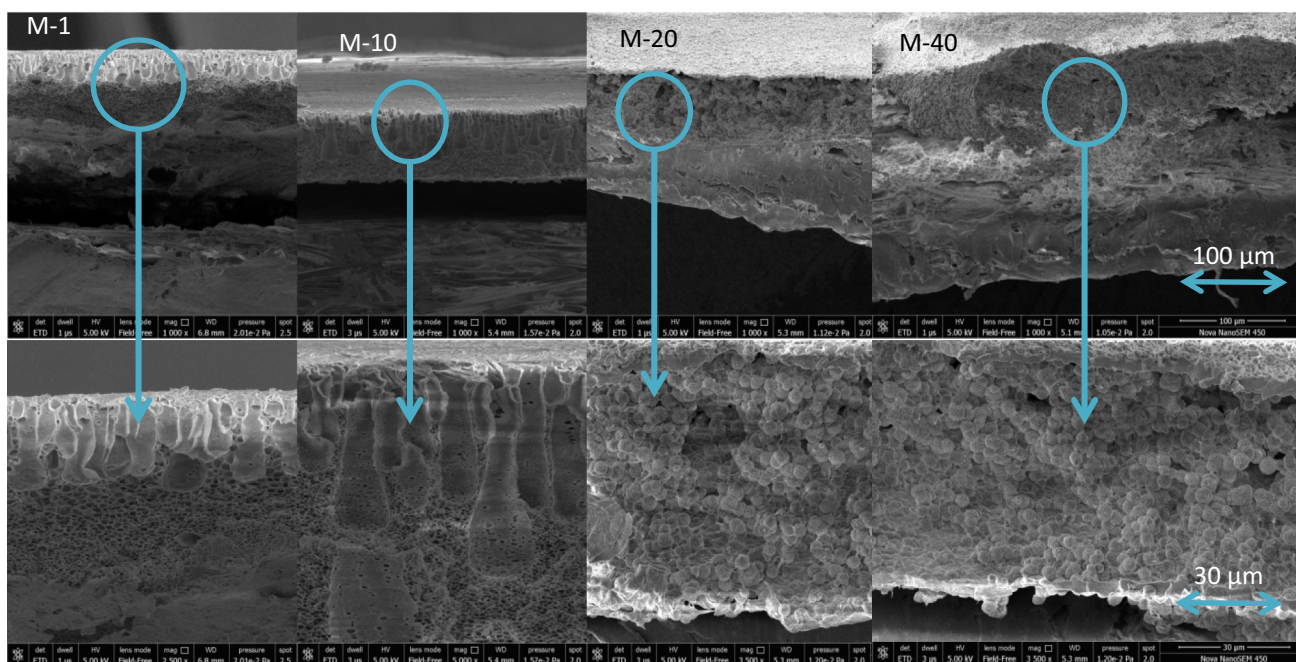


Fig. 2 SEM images of the cross-sectional surface of PVDF membrane prepared with different EIPS evaporation times at 1000 X (top) and 5000 X (bottom) magnification

nature with a small thin polymeric layer at the top surface, showing that for EIPS evaporation time 10 min only, the surface of the membrane get affected, whereas the membrane matrix is similar to that prepared by NIPS method.

On further increasing the EIPS evaporation time for the membrane to 20 and 40 min, the membrane morphology underwent dramatic changes. The top surface is rough and porous with spherulitic micro-particles are linked together through fiber-like connections. This implies that polymeric film may precipitate, and PVDF particles aggregate due to crystallization during the slow phase separation process induced by water vapors present in the environment. Here, the crystallization of PVDF (solid–liquid demixing) has become a competitive and predominant phase separation mechanism compared to liquid–liquid demixing during phase separation. The cross-section representation of this membrane is shown in Fig. 2. It can be easily illustrated from the micrographs that globular particles are created and interlocked totally to form an open bi-continuous network. The same behavior in the top and cross-sectional microstructure is observed for M-3 and M-4. This indicates homogeneous and symmetric morphology throughout the membrane matrix. For a long exposure time, the demixing is initiated before immersion into the coagulation bath, which results in globular morphology without cellular pores.

The synthesized membrane's average pore size is depicted in Fig. 3, aligning with the described formation process. Initially, at a 1-min evaporation time, the pore size measured 0.13 μm . Subsequently, as the evaporation time increased

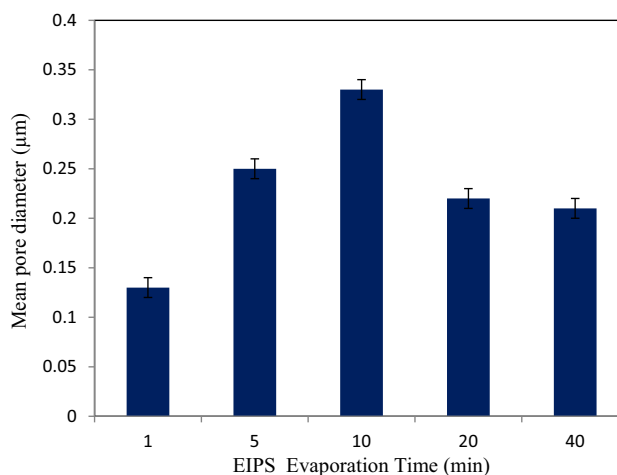


Fig. 3 Effect of EIPS time on Average pore diameter of fabricated membrane

to 10 min, the pore size expanded to 0.33 μm . However, at a 40-min evaporation time, the pore size decreased to 0.21 μm . These findings indicate that during the first 10 min, the Non-Solvent Induced Phase Separation (NIPS) process predominates over the Evaporation-Induced Phase Separation (EIPS) processes, resulting in an overall asymmetric membrane structure created through the NIPS method. Nonetheless, a minor alteration at the top layer contributes to an increase in the membrane's hydrophobicity. Furthermore, with further increases in time, the EIPS process surpasses the

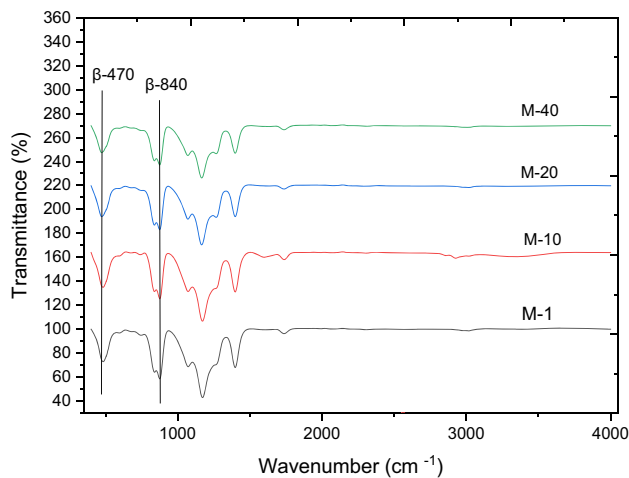


Fig. 4 FTIR spectra of membranes M-1 to M-40 in the range of 400–4000 cm^{-1}

phase inversion process, resulting in a symmetrical membrane with smaller pore sizes. Dehban (2021) documented analogous results, highlighting that the membrane aperture displayed a sequence of behaviors: it initially expanded, subsequently contracted, as exposure time prolonged [22].

3.3 Effect on the Crystal Structure of PVDF Membranes

The FTIR spectrum analysis was performed to investigate the change in the specific crystalline phase of different membranes M-1 to M-40 on increasing the evaporation time of EIPS process during phase inversion. The transmittance represented in FTIR spectra of fabricated membranes under various evaporation times is shown in Fig. 4 for wave number range from 400 to 4000 cm^{-1} . It is observed that a similar trend of depression was followed by all four membranes. It is also corroborated from the spectra that β phase polymerization dominates over the other two-phase (α and γ) since depression in each spectrum is observed to be at 840 and 470 cm^{-1} . However, the depression peak is not observed at 796 and 762 cm^{-1} for α phase and 834, and 567 cm^{-1} for γ phase polymerization—this occurrence of β polymerization because of the use of polar solvent for membrane synthesis. β polymorphs show high dipole movement as they align with the same direction of C-F bonds of polar solvent whereas α polymorphs show zero dipole movement as they are oriented in opposite directions. Generally, α polymorphs are favored during the crystallization of PVDF polymer, but β polymorphs are more stable thermodynamically. Moreover, the EIPS process makes the membrane formation process slower which favors thermodynamically stable β polymorph as compared to faster NIPS process. Cui. Z. (2015) reached a similar conclusion, indicating that a higher concentration

of the solution promotes the formation of the β phase of polymerization [23]. Furthermore, as the duration of exposure to EIPS increases, the remaining polymeric solution becomes more concentrated. Consequently, with prolonged EIPS exposure, the dominance of β phase polymerization over the other two phases becomes more pronounced.

3.4 Study of Membrane Hydrophobicity and Topography

The membrane wetting phenomena is understood by estimating the contact angle and LEP of the synthesized membranes. It is found that the membrane contact angle increased from 91° to 117°, along with the increase in LEP from 19 to 180 kPa on increasing the EIPS evaporation time from 1 to 40 min, as shown in Figs. 5 and 6 respectively. It is also evident from the figure that the desired contact angle was obtained at an evaporation time of 10 min with a suitable LEP for the membrane distillation process. The cause of the increase in contact angle and LEP may be attributed to the fact that a membrane with a short exposure time may create a smooth top surface compared to a higher exposure time. This fact is further examined by the AFM topography, as shown in Fig. 7 to investigate the surface roughness [24]. It is visualized that at a lower time EIPS evaporation of 1 min, the surface roughness is found to be 81 with 38.6 nm (ridge) and -42.4 nm (valley) as compared to the surface roughness of 229 and 725.9 nm for 10 and 20 min, respectively. Henceforth, the surface roughness is minor at a lower evaporation time. This supports the fact of increasing contact angle with evaporation time. Moreover, in this study, the increment in contact angle and surface roughness was observed on increasing evaporation time. This can be understood by the fact that liquid–liquid de-mixing mass transfer trends shift towards solid–liquid de-mixing.

3.5 Membrane Porosity and Its Mechanical Properties

The effect of EIPS on membrane porosity and its mechanical properties are represented in Fig. 8. On increasing the EIPS time from 1 to 40 min, the synthesized membrane porosity decreases from 58.7 to 52.3%. The decrement in the porosity is due to the phase separation process prevailing before coagulation because of solid–liquid demixing at a higher evaporation time. As a result, polymer agglomerates form worm-like structures, which in turn create smaller pore sizes and poor interconnectivity in the synthesized PVDF membrane. The same can also be corroborated from the SEM image as shown in Figs. 1 and 2.

At lower evaporation time, there is a rapid exchange of solvent and non-solvent at the membrane interface during coagulation. This is because of the reason that the chemical

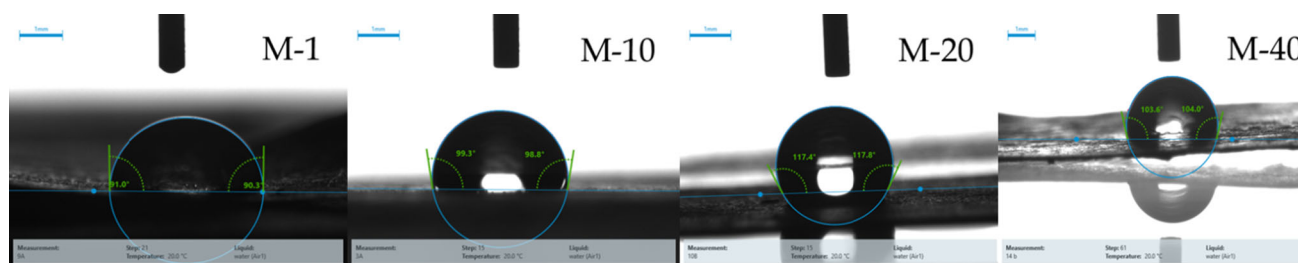


Fig. 5 Contact angle of prepared membranes with varying EIPS evaporation time

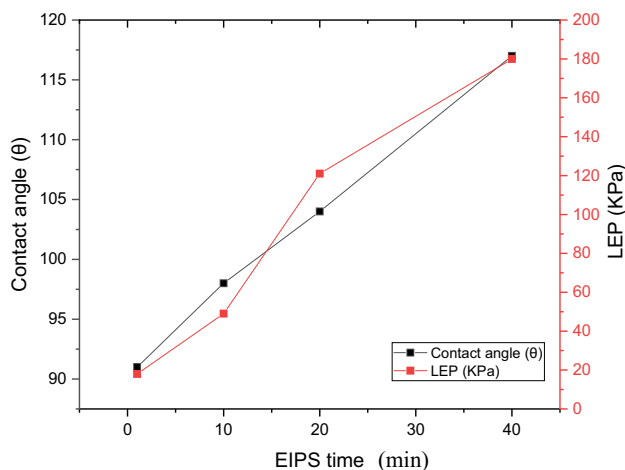


Fig. 6 Effect of EIPS evaporation time on contact angle and LEP of synthesized membranes

composition of the thin polymeric layer at the membrane's top surface is above the binodal line in the ternary phase diagram. In contrast, the chemical composition of the membrane matrix is below the binodal line at the time of phase inversion. This phenomenon creates a smooth top surface and deeper finger-like pores in the membrane matrix. Furthermore, the developed polymeric skin layer acts as a mass-transfer barrier between solvent and non-solvent and increases the time for exchange of solvent and non-solvent, which results in the asymmetric highly porous structure of the membrane at lower evaporation time. In spite of the bigger average pore size of the membrane at the surface for the membrane prepared with an EIPS evaporation time of 10 min, its porosity decreases as the length of finger-like pores decreases. In EIPS process, non-solvent moves in the upward direction of the membrane matrix because of the concentration gradient formed on the membrane surface. So, the fraction of solvent decreases in the membrane matrix at the time of the NIPS process, causing in reduction of the size of finger-like pores (caused by instantaneous de-mixing). The decrement in the void fraction of the membrane matrix results in a less porous membrane and on further increasing the EIPS evaporation time, nucleation and growth process dominates over the NIPS process, i.e.,

most of the solvent from the membrane matrix gets evaporated before putting it into the coagulation bath favoring the spherulites formation by nucleation and growth mechanism. The structure of the membrane became symmetrical with less void content resulting in a decrement in porosity.

Moreover, the tensile strength of the fabricated membrane was estimated using UTM under various evaporation times. Figure 8 implies that membrane tensile strength decreases from 180 to 117 MPa on increasing the EIPS time from 1 to 40 min. The reason for declining tensile strength may be attributed to the fact that at higher EIPS time, the polymer matrix is not interconnected due to extreme solid-liquid demixing. This creates polymer agglomeration throughout the membrane matrix, as a result, a worm-like structure and less flexible microstructures are formed. In the literature [24, 25], it was emphasized that with a decrease in membrane porosity, the membrane tensile strength increases, however, an exciting result was observed in this study that both membrane porosity and its tensile strength decrease. Zhao (2018) contended that the emergence of spherulites within the membrane matrix leads to a reduction in membrane strength [26]. Consequently, in a similar vein, as the EIPS time increases, spherulite formation takes precedence. Despite a decrease in porosity, it's worth noting that membrane tensile strength also declines. This result shows that membrane porosity and tensile strength may show antagonistic as well as synergistic effects depending on the interconnectivity of polymer matrix during membrane fabrication.

3.6 Flux Through the Membrane

The fabricated PVDF membranes were tested for desalination through the VMD process, line diagram of which is illustrated in Fig. 9. The feed solution of 20,000 mg/l NaCl concentration was taken in a feed tank of 10 L. This highly concentrated solution was heated at 60 °C and feed with a volumetric flow rate of 2 lpm to the membrane module of an effective membrane diameter of 52 mm under permeate pressure of 10 kPa. The excess solution was bye-passed to the feed tank. The vapor emerging in the permeate channel of the membrane module was condensed in the condenser

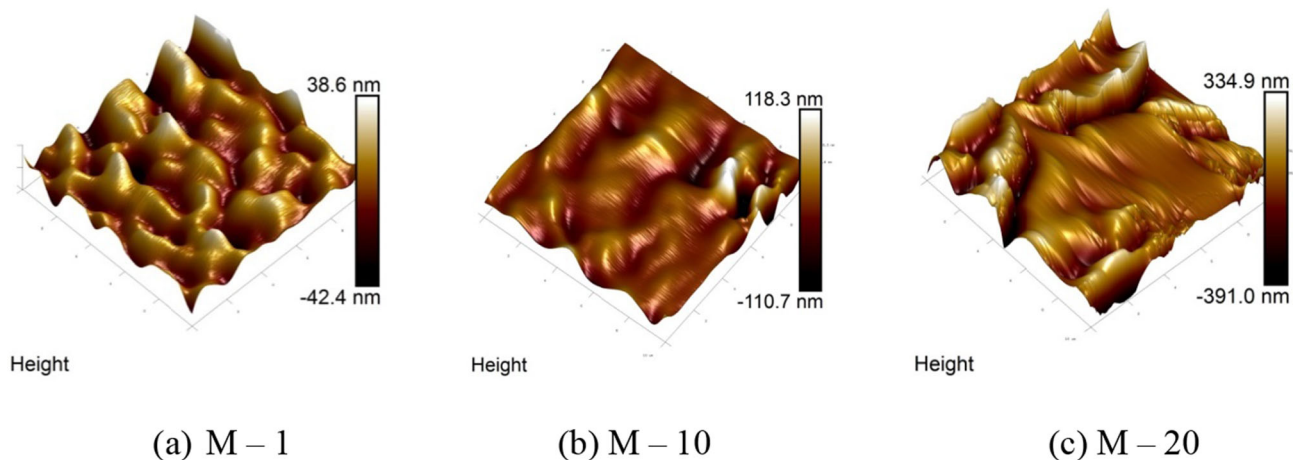


Fig. 7 AFM images of the top surface morphology for membranes M-1, M-10, and M-20

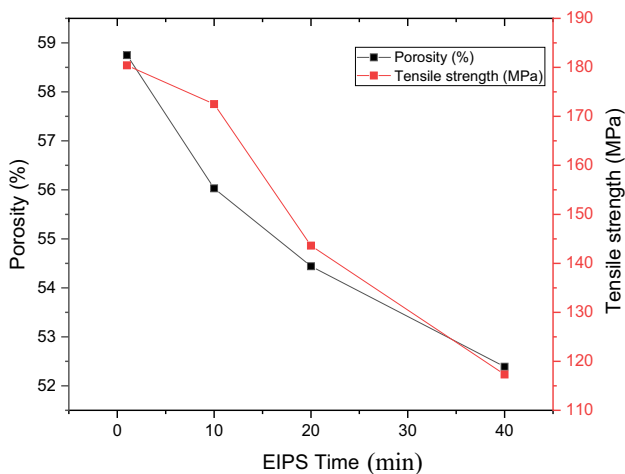


Fig. 8 Effect of EIPS time on porosity and tensile strength

using a continuous supply of cold water from the chiller in which the temperature was maintained at 10 °C.

The water permeates flux obtained under stable operating conditions for various fabricated membranes with respect to EIPS evaporation time is shown in Fig. 10. It is observed from the figure that the highest permeate flux of 12.8 kg/m²h was obtained at EIPS evaporation time of 10 min. This is because of Poiseuille contribution along with Knudsen diffusion (0.01 < Kn < 1). Knudsen number is estimated to be 0.6 at STP by Eq. 8 as follows:

$$Kn = \frac{\lambda}{d_{pore}} = \frac{1}{\sqrt{2\pi} d_w^2 \frac{N}{V}} \tag{8}$$

where, λ is the mean free path of the water vapor molecule transferred (m), d_w is water vapor molecule diameter (m), N/V is the number of molecules per unit volume (m⁻³), d_{pore} is the mean pore diameter of the membrane (m).

Mean pore diameter is highest for EIPS evaporation time of 10 min, therefore, the permeate flux is also highest for this evaporation time since flux is proportional to d_{pore}² for Poiseuille flow. The superior quality of the membrane prepared under these conditions is due to optimal solvent uptake. However, with a further increase in exposure time for the EIPS process, the flux decreases. This decline in permeate flux is because of significant changes occurring in the microstructure of the fabricated membrane since the finger-like structure of the membrane converted to a worm-like morphology on increasing the EIPS time from 10 to 40 min. Moreover, the surface roughness is also increased at higher EIPS time; as a result membrane hydrophobicity gets enhanced, which can be attributed to a higher contact angle. The percentage removal is found to be constant throughout under the range 99.3–99.9% with all the fabricated membranes under different EIPS evaporation time.

3.7 Fouling Study

In a continuous operation, the salt concentration of 20,000 ppm was used as a feed solution for a VMD setup and the trans membrane permeate flux was collected continuously for about 200 h for all the four synthesized membrane at various EIPS time to understand the fouling phenomena. The operating conditions of the VMD setup were kept constant throughout the operation: 20,000 ppm of NaCl feed solution, 60 °C of feed temperature, 2 lpm of feed flow rate, and 10 kPa of vacuum pressure for 200 h run. From Fig. 11, it was observed that there is no significant decline in the permeate flux for all the four membranes within 200 h process duration. The permeate flux was found to be in the range of 14.89–13.8 kg/m² h for membrane synthesized at 10 min EIPS time. However, permeate flux was in the range of 11.49–10.7 kg/m² h, 10.56–9.69 kg/m² h and

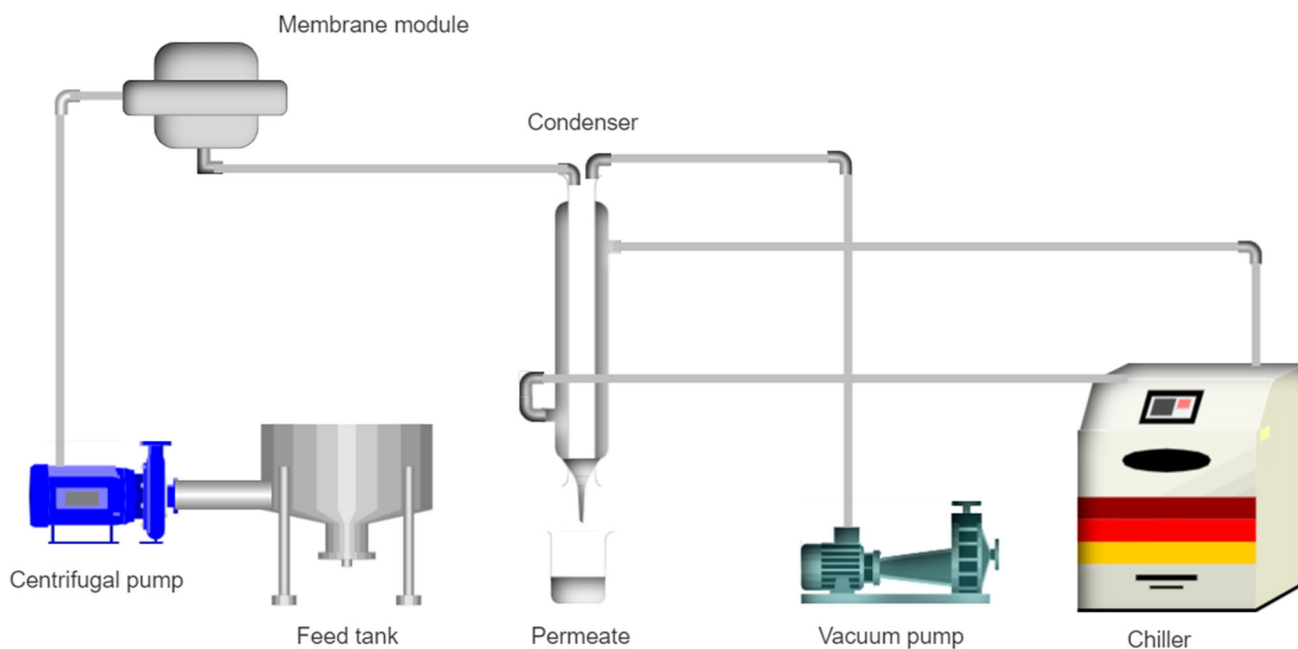


Fig. 9 Pictorial representation of vacuum membrane distillation unit

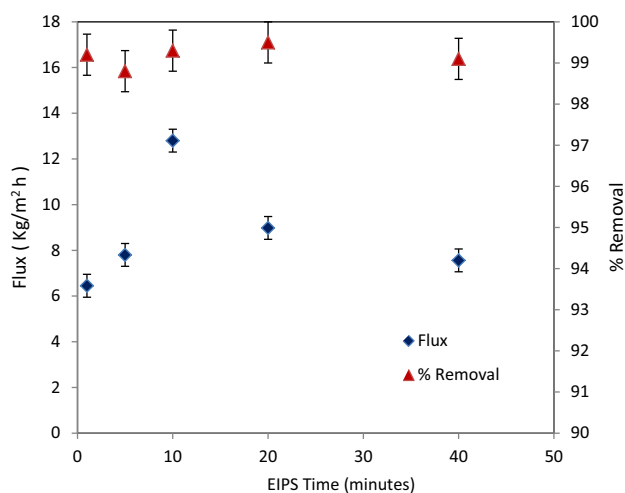


Fig. 10 Effect of EIPS time on VMD Flux and % Removal

9.54–8.79 kg/m² h for the synthesized membrane at 20, 40 and 1 min of EIPS. Sing et al. observed comparable findings when utilizing a commercial PVDF membrane. They noted a 4% reduction in permeate flux through the membrane over a continuous operation period of 200 h [27]. This minimal decrement during the process may be due to the minor scale deposition on the membrane surface. Each experiment is conducted twice and the average value is considered in the data.

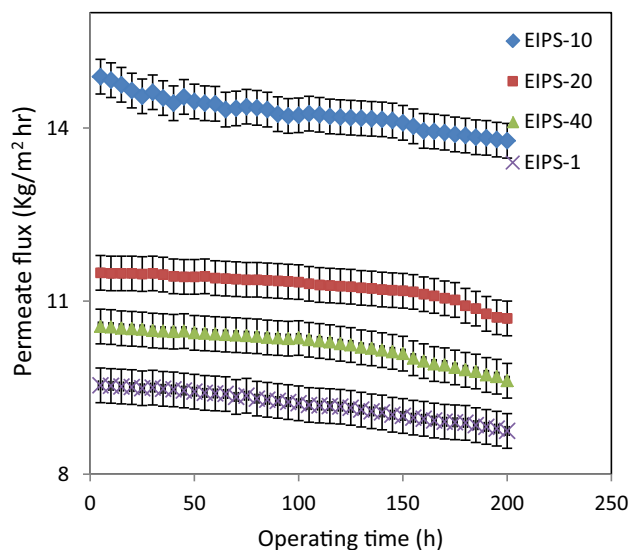


Fig. 11 Effect of operating time on the permeate flux of synthesized membranes

4 Conclusion

In this study, PVDF microporous hydrophobic membranes were fabricated by combining two-phase inversion techniques in order to modify the properties of PVDF membrane

for desalination application using Vacuum Membrane Distillation. It was found from the micrographs that the membrane microstructure changes remarkably from an asymmetrical structure with finger-like long deep pores followed by sponge-like pores to a worm-like structure throughout the membrane matrix on increasing the evaporation time from 1 to 40 min. Furthermore, it was also observed that membrane surface roughness gets affected significantly from 38.6 to 334.9 nm on increasing the evaporation time from 1 to 20 min. These elevations of ridges at higher evaporation times also increase the membrane contact angle to a great extent. The FTIR spectroscopy of membrane corroborated that during phase inversion, β polymerization dominates the α and γ type polymerization. The pore size of membrane is greatly affected by the EIPS evaporation time and at 10 min evaporation time, maximum mean pore diameter was obtained (0.33 μm) despite a slight decrease in porosity. The membrane prepared with evaporation time of 10 min shows better performance with 12.8 $\text{kg/m}^2\text{h}$ flux through VMD with expectable LEP of 49 kPa with a good hydrophobicity characteristics of contact angle 98°. All fabricated membranes were rigorously tested within the VMD setup for desalinating highly concentrated NaCl solutions. The results demonstrated the membrane's high potential for desalination, as the percentage removal consistently ranged from 99.3 to 99.9% across membranes prepared under varying EIPS times. Furthermore, fouling phenomena during VMD operation has been investigated in long run. It is clearly evident from the experimentation that fabricated membrane under 10 min evaporation time exhibits negligible fouling compared to others. Even after a 200-h continuous run. In conclusion, the integration of EIPS alongside NIPS in membrane fabrication offers a promising avenue for achieving excellent hydrophobicity, controlled pore size, enhanced flux, and superior performance during continuous operations. This study underscores the potential for tailoring membrane properties to meet the specific demands of VMD-based desalination applications."

References

1. L Zheng Z Wu Y Wei Y Zhang Y Yuan 2016 Preparation of PVDF-CTFE hydrophobic membranes for MD application: effect of LiCl-based mixed additives J. Memb. Sci. 506 71 85 <https://doi.org/10.1016/j.memsci.2016.01.044>
2. G Dong Kang Y Ming Cao 2014 Application and modification of poly(vinylidene fluoride) (PVDF) membranes-a review J. Memb. Sci. 463 145 165 <https://doi.org/10.1016/j.memsci.2014.03.055>
3. EU Khan AR Martin 2014 Water purification of arsenic-contaminated drinking water via air gap membrane distillation (AGMD) Period. Polytech. Mech. Eng. 58 1 47 53 <https://doi.org/10.3311/PPme.7422>
4. R Baghel S Upadhyaya SP Chaurasia K Singh S Kalla 2018 Optimization of process variables by the application of response surface methodology for naphthol blue black dye removal in vacuum membrane distillation J. Clean. Prod. 20 199 900 915 <https://doi.org/10.1016/j.jclepro.2018.07.214>
5. Y Liao CH Loh R Wang AG Fane 2014 Electrospun superhydrophobic membranes with unique structures for membrane distillation ACS Appl. Mater. Interfaces 6 18 16035 16048 <https://doi.org/10.1021/am503968n>
6. PTP Aryanti 2021 Preparation of Polypropylene/PVDF Composite Membrane by Dip-Coating Method IOP Conf. Ser. Mater. Sci. Eng. 1115 1 012028 <https://doi.org/10.1088/1757-899x/1115/1/012028>
7. MA Tofighy T Mohammadi MH Sadeghi 2021 High-flux PVDF/PVP nanocomposite ultrafiltration membrane incorporated with graphene oxide nanoribbons with improved antifouling properties J. Appl. Polym. Sci. 138 4 1 15 <https://doi.org/10.1002/app.49718>
8. H Junoh 2021 Porous polyether sulfone for direct methanol fuel cell applications: Structural analysis Int. J. Energy Res. 45 2 2277 2291 <https://doi.org/10.1002/er.5921>
9. D Kamarudin N Awanis Hashim BH Ong Y Kakihana M Higa H Matsuyama 2021 Multiple effect of thermal treatment approach on PVDF membranes: Permeability enhancement and silver nanoparticles immobilization J. Environ. Chem. Eng. 9 4 105769 <https://doi.org/10.1016/j.jece.2021.105769>
10. PK Prajapati 2021 Increase of flow-through pores in rationally designed organosilica-PVDF nanocomposite membrane J. Appl. Polym. Sci. 138 34 1 10 <https://doi.org/10.1002/app.50846>
11. X Wang 2023 Preparation of lateral flow pvdf membrane via combined vapor- and non-solvent-induced phase separation (V-NIPS) Membr. (Basel) <https://doi.org/10.3390/membranes13010091>
12. C Meringolo TF Mastropietro T Poerio E Fontananova G Filpo De E Curcio G Profio Di 2018 Tailoring PVDF membranes surface topography and hydrophobicity by a sustainable two-steps phase separation process ACS Sustain. Chem. Eng. 6 8 10069 10077 <https://doi.org/10.1021/acssuschemeng.8b01407>
13. NI Mat Nawi HM Chean N Shamsuddin MR Bilad T Narkkun K Faungnawakij AL Khan 2020 Development of hydrophilic PVDF Membrane using vapour induced phase separation method for produced water treatment Membranes 10 6 121
14. S Ohno I Nakata R Nagumo K Akamatsu X Lin Wang S Ichi Nakao 2021 Development of low-fouling PVDF membranes blended with poly(2-methoxyethyl acrylate) via NIPS process Sep. Purif. Technol. <https://doi.org/10.1016/j.seppur.2021.119331>
15. C. M. Hansen, "The three dimensional solubility parameter and solvent diffusion coefficient. Their importance in surface coating formulation," *J. Paint Technol.*, p. 104, 1967.
16. H Rabiee A Ghadimi T Mohammadi 2015 Gas transport properties of reverse-selective poly(ether-b-amide6)/[Emim][BF4] gel membranes for CO₂/light gases separation J. Memb. Sci. 476 286 302 <https://doi.org/10.1016/j.memsci.2014.11.037>
17. J Phattaranawik R Jiratananon AG Fane 2003 Heat transport and membrane distillation coefficients in direct contact membrane distillation J. Memb. Sci. 212 1–2 177 193 [https://doi.org/10.1016/S0376-7388\(02\)00498-2](https://doi.org/10.1016/S0376-7388(02)00498-2)
18. J Phattaranawik R Jiratananon AG Fane 2003 Effect of pore size distribution and air flux on mass transport in direct contact membrane distillation J. Memb. Sci. 215 1–2 75 85 [https://doi.org/10.1016/S0376-7388\(02\)00603-8](https://doi.org/10.1016/S0376-7388(02)00603-8)
19. BB Ashoor S Mansour A Giwa V Dufour SW Hasan 2016 Principles and applications of direct contact membrane distillation (DCMD): A comprehensive review Desalination 398 222 246 <https://doi.org/10.1016/j.desal.2016.07.043>
20. JS Lee HH Lee JA Seo HS Park J Park BR Min 2015 Interfacial polymerization on hydrophobic PVDF UF membranes surface: Membrane wetting through pressurization Appl. Surf. Sci. 356 1207 1213 <https://doi.org/10.1016/j.apsusc.2015.08.226>



21. TA Agbaje S Al-Gharabli MO Mavukkandy J Kujawa HA Arafat 2018 PVDF/magnetite blend membranes for enhanced flux and salt rejection in membrane distillation *Desalination* 436 69 80 <https://doi.org/10.1016/j.desal.2018.02.012>
22. D Amin FH Saeedavi A Kargari 2022 A study on the mechanism of pore formation through VIPS-NIPS technique for membrane fabrication *J. Ind. Eng. Chem.* 108 54 71 <https://doi.org/10.1016/j.jiec.2021.12.023>
23. Z Cui NT Hassankiadeh Y Zhuang E Drioli YM Lee 2015 Crystalline polymorphism in poly(vinylidene fluoride) membranes *Prog. Polym. Sci.* 51 94 126 <https://doi.org/10.1016/j.progpolymsci.2015.07.007>
24. F Shi Y Ma J Ma P Wang W Sun 2012 Preparation and characterization of PVDF/TiO₂ hybrid membranes with different dosage of nano-TiO₂ *J. Memb. Sci.* 389 522 531 <https://doi.org/10.1016/j.memsci.2011.11.022>
25. F Wang 2014 Physical modification of polytetrafluoroethylene flat membrane by a simple heat setting process and membrane wetting remission in SGMD for desalination *Desalination* 354 143 152 <https://doi.org/10.1016/j.desal.2014.09.030>
26. Q Zhao 2018 Preparation of high strength poly(vinylidene fluoride) porous membranes with cellular structure via vapor-induced phase separation *J. Memb. Sci.* 549 151 164 <https://doi.org/10.1016/j.memsci.2017.10.068>
27. JK Singh S Upadhyaya SP Chaurasia R Baghel 2017 Study on membrane fouling in vacuum membrane distillation for desalination *J. Basic Appl. Eng. Res.* 4 229 233

Springer Nature or its licensor (e.g. a society or other partner) holds exclusive rights to this article under a publishing agreement with the author(s) or other rightsholder(s); author self-archiving of the accepted manuscript version of this article is solely governed by the terms of such publishing agreement and applicable law.